

STUDY OF GRAVITATIONAL TURBULENT MIXING AT LARGE DENSITY DIFFERENCES USING DIRECT 3D NUMERICAL SIMULATION

Yu.V.Yanilkin, V.P.Statsenko, S.V.Rebrov, O.G.Sin'kova, A.L.Stadnik

Paper to be presented at the 8th International Seminar on Turbulent Mixing of Compressible Matter (8th IWPCTM, Pasadena, USA)

The problem of turbulent mixing under action of a constant gravity force (constant acceleration) on a plane interface of two gases was numerically studied by a number of papers [1, 2], however the studies are essentially missing for large density differences in mixing materials.

This paper makes an attempt of direct 3D numerical simulation of the above problem with code TREK [3] for gases of different densities, such that $n=\rho_2/\rho_1=3-40$. With these density differences, the numerical simulations involve severe difficulties in achievement of the self-similar regime of a turbulent flow, so the difference scheme and the number of the computational cells were varied in the computations. A large number of the computations were conducted, it is impossible to demonstrate results of all the computations, however, note that the results agree well with each other. Below are results of computations by the same difference scheme and on the same computational grid.

Numerical arrays of hydrodynamic quantities from 3D computations are used to find moments of the quantities (Reynolds tensor, turbulent flows, profiles of density and its mean square pulsation). Besides, they are also used for construction of one-point concentration probability density function (PDF). Spectral analysis of velocity and density pulsations in TMZ was conducted: the effect on the approximation to the Kholmogorov spectrum for the quantities was studied.

The computed data is compared to known experimental data [4-9]. The analysis of the computed and experimental data suggests that the flow is not self-

similar at the initial quite long stage, and the stage should be excluded to when determining the well-known self-similar constant α . In view of this it seems to us that most experimental data need to be corrected.

1. Setting up TREK computations

The problem is formulated similar to ref. [1]: at the initial time two half-spaces separated with plane $z=z_c=0$ are filled with ideal gases in rest having densities $\rho_1=1$ и $\rho_2=n$ ($n=3, 10, 20, 40$). The initial geometry is presented in Fig.1. The gravitational acceleration, $g_z = -1 \equiv -g$, is directed from the heavy material to the light. At the initial time, at the interface (in a layer one cell thick), a random-number generator gives random density perturbations $\delta\rho = \pm \rho_1\delta$, where $\delta=0.1$.

Gas dynamics equations for ideal two-component medium (with zero molecular viscosity and heat conduction) are solved. The computational domain is a parallelepiped with height $\Lambda=2$. Its horizontal face is a square with side $L_x=L_y=1$.

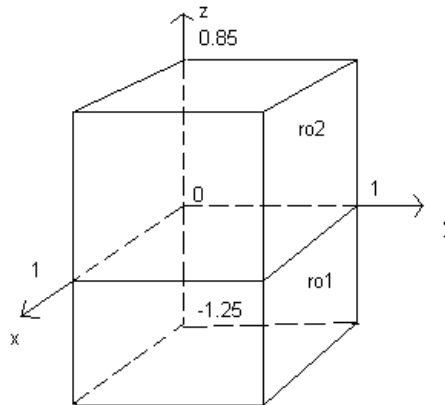


Fig.1. Initial geometry

The initial pressure profile was given using the hydrostatic equilibrium

condition $p(z) = p_0 - \int_{z_2}^z \rho(z) \cdot g \cdot dz$. Here the coordinate of the upper face is

$z_2=0.85$, that of the lower face $z_1= -1.15$, $p_0=100$. Note that the pressure ($p \approx p_0$)

is such, that the following non-compressibility condition was met well for the turbulent flow $k=\xi L_t g \ll \gamma p/\rho$, where $\xi=\text{const} \ll 1$, $L_t < \Lambda$, L_t is turbulent mixing zone (TMZ) width, k is turbulent energy.

The equation of state is ideal gas with adiabatic constant $\gamma=1.4$. The computational grid is uniform, having $N_x=200$, $N_y=200$, $N_z=400$ cells. The ‘‘rigid wall’’ type condition was posed on all the computational domain boundaries.

2. Results of 3D computations, integral characteristics

The flow evolution observed in all the computations is similar on the whole to the previous computations [2] for small density differences: whirl enlargement with time and change over to the self-similar regime are observed.

The latter shows up for this problem, in particular, as transition to the linear dependence of TMZ width function $L_t(t)$:

$$F \equiv \frac{1}{t_L} \sqrt{\frac{L_t}{Ag}}. \quad (1)$$

Here the unit of measurement for time is $t_L \equiv \sqrt{\frac{L_x}{g}}$ and $L_t(t)$,

$$L_t \equiv z_2 - z_1, \quad (2)$$

is TMZ width along z determined by points z_1, z_2 , at which quite small value of ε of a hydrodynamic quantity, for example, concentration, is achieved. Next, assume that $c_2(z_1)=\varepsilon$, $c_2(z_2)=1-\varepsilon$, where c_2 is mass fraction of the material whose initial density was $\rho_2 = n$.

The angle of inclination, dF/dt , therewith determines the value of coefficient $\alpha_a=(dF/dt)^2$ in the relation for the TMZ width at the self-similar stage:

$$L_{ta} = \alpha_a Agt^2. \quad (3)$$

Fig. 2 plots $F(t)$ from the computations using relations (1) and (2).

For $n=8.5-29$, the α_a obtained in the experiments [7] range from 0.15 to 0.2 and slightly increase with increasing n . The relevant straight lines also appear in Fig.2.

As seen from Fig.2, there are two flow segments differing in the angle of inclination dF/dt , at the initial segment this is larger than in the experiment, at the second segment this is, on the contrary, less. Prior to us, similar results were obtained by Youngs [1]. A comprehensive analysis of the flow suggests that at the first segment there is no flow self-similarity, although the inclination dF/dt is close to constant. The self-similarity takes place only at the second stage, therefore it is this segment that the self-similar constant α should be measured at, where it proves less than the known experimental data. We assume, that it is caused by that at processing the specified data was not excluded initial nonself-similar a stage.

What this can result in can be seen from the experimental data of Kucherenko et al., which we analyzed.

Fig.3 plots function $F_2(t) \equiv \frac{1}{t_L} \sqrt{\frac{z_2 - z_c}{Ag}}$ versus time for coordinate z_2 of

the penetration of the heavy liquid into the light. At the final stage, where the self-similar regime is achieved, our computation for $n=40$ results in the angle of inclination dF_2/dt close to the observed: Fig.3 presents minimum and maximum quantities measured in [9] for $n=36.5$. Note that by $\alpha_2=0.078$ ($\alpha_2=(dF_2/dt)^2$) taken in [9] the angle of inclination is larger than the observed. Apparently, this value was obtained without exclusion of the initial segment, at which the self-similarity also does not take place.

A similar dependence for smaller density differences is shown in Fig.4. Apparently, the self-similar regime is not achieved in the experiment (for $n=3.65$): the angle of inclination decreases about in the same manner as in our computation (for $n=3$) at the initial stage, where the self-similar regime is not also achieved. In [9] $\alpha_2=0.078$, this is significantly higher than the observed and corresponds just to the initial (non-self-similar) stage.

Fig.5 plots the scaled TMZ width:

$$\alpha(t) = \frac{L_t}{Ag(t-t_0)^2}, \quad (4)$$

that follows from our computations. Here t_0 corresponds to the intersection of the extrapolated self-similar segment of curve $F(t)$ estimated by the data of Fig. 2 with the abscissa axis.

In the computations with $n=10, 20, 40$, α approaches approximately constant values (which corresponds to the self-similar stage): $\alpha_a \approx 0.11, 0.15, 0.16$, respectively, which is somewhat less than the experimental quantities [8]. Note that the self-similar stage is achieved earlier with increasing n , but its duration becomes shorter.

Processing similar to (4) was performed for coordinates z_1, z_2 of the penetration of the heavy liquid into the light and the light into the heavy, respectively. Their scaled values are

$$\alpha_1 \equiv \frac{z_c - z_1}{Ag(t - t_0)^2}, \quad \alpha_2 \equiv \frac{z_2 - z_c}{Ag(t - t_0)^2} \quad (5)$$

The results are plotted in Fig.6. On the whole, $\alpha_1(t), \alpha_2(t)$ behave like $\alpha(t)$. In so doing, as might be expected, TMZ grows faster toward the light material. Asymmetry increases with increasing n and reaches ≈ 2 for $n=40$.

For this problem the self-similar regime also shows up by the fact that the following quantity becomes time-independent:

$$E(t) \equiv \frac{k_m}{L_t g}, \quad (6)$$

where $k_m(t) \equiv \max(\langle k \rangle(z, t))$ is maximum averaged turbulent energy over the TMZ width:

$$k(z) = \frac{\langle (u_j)^2 \rangle - \langle u_j \rangle^2}{2}, \quad (7)$$

the averaging (denoted with $\langle \rangle$) is over the entire horizontal section $z = \text{const}$.

As seen from Fig.7, at the initial stage $E(t)$ is large enough [at this stage, there is a small number of computational cells per TMZ, which leads to insufficiently correct values of $E(t)$] and increases with increasing n in all the computations. At a later stage this quantity approaches approximately constant $E = E_a$ in the computations with $n=3, n=10$, and $n=20$. The E_a also increases with increasing n .

To draw a more justified conclusion about whether or not the self-similar regime is achieved, other turbulent quantities have to be considered.

The TMZ maximum value, R_m , of density pulsation function R versus time is plotted in Fig.7,

$$R_m \equiv \max(R), \quad R \equiv \frac{\langle \rho'^2 \rangle}{\rho^2}. \quad (8)$$

From the figure it is clear that at the self-similar stage the R_m quite confidently approaches approximately constant $R_m \approx R_a$ in all the computations. The R_a increases with increasing n .

Fig.9 plots the TMZ maximum turbulent mass flow versus time:

$$R_{zm} \equiv \max(\tilde{R}_z), \quad \tilde{R}_z \equiv \frac{R_z}{\sqrt{L_t g}}, \quad R_z \equiv \langle \rho' u'_z \rangle \quad (9)$$

Like for the R_m , from Fig.9 it follows that at the self-similar stage the R_{zm} approaches approximately constant $R_{zm} \approx R_{zma}$ increasing with increasing n .

Thus, the analysis shows that at the initial flow stage the self-similar regime is not established and this segment should be excluded when considering self-similar flow characteristics. This is also true for the experiments, in which initial perturbations able to affect the flows under study for long are always present.

3. Velocity and density pulsation spectra

The computed data was used as a basis to study the velocity pulsation spectrum according to relation

$$\begin{aligned} E_{iil}^{(s)}(x, y) &= \langle u_i^2 \rangle_{|l, x, y, z} - \langle u_i \rangle_{|l, x, y, z}^2 \quad ; \quad s = 1, 2, \dots, N_z \\ E_{iil}(z) &= E_{iil}^{(s)} = \langle E_{iil}^{(s)}(x, y) \rangle \quad ; \quad l = rh, \quad r = 2, 3, \dots, N_x. \end{aligned} \quad (10)$$

Here averaging $\langle \rangle_{|l, x, y}$ is performed in the s -layer (over z) in a square with side l ($l=rh$, h is computational cell size), whose center coordinates are x, y , and then averaging $\langle \rangle$ is made over all possible values x, y of the squares with the l in the entire s -th layer. In (10) there is no summation over i .

Next:
$$E_1 = \sum_{i=1}^{i=3} E_{iil} \quad (11)$$

Fig. 10 plots the results of the computation for $t=2$, $n=40$ (where $K=2\pi/l$) along with Kolmogorov spectrum

$$\lg E_1 = -2K/3 + \text{const.} \quad (12)$$

Inside the TMZ ($|\zeta| \leq 0.3 \div 0.4$; $\zeta \equiv \frac{z - z_c}{L_t}$, here L_t was computed by model [2]), the computed spectrum of total energy E_1 approaches the 3D Kolmogorov spectrum, with this being less confidently for highest n . Fig. 10 also shows that at small space scales (large K) the velocity pulsations become isotropic: all components E_{iil} approach each other.

A similar quantity is calculated for the squared density pulsations:

$$\begin{aligned} \rho_l^s(x, y) &= \langle \rho^2 \rangle_{|l,x,y,z} - \langle \rho \rangle_{|l,x,y,z}^2 \quad ; \quad s = 1, 2, \dots, N_z \\ \rho_l(z) &\equiv \langle \rho_l^s(x, y) \rangle \quad ; l = rh, \quad r = 2, 3, \dots, N_x; \end{aligned} \quad (13)$$

this is depicted in Fig. 11. As seen, at the TMZ center the spectrum of net ρ_l at small scales approaches the Kolmogorov spectrum. In contrast to the velocity pulsation spectrum, the density pulsation spectrum is closer to the Kolmogorov spectrum with increasing n .

4. Concentration probability density function

The one-point heavy material mass concentration probability density function was determined by the computed data:

$$F(c_2, z, t) = \frac{N(c_1^{(ik)}(z) \geq c_2) - N(c_2^{(ik)}(z) \geq (c_2 + \Delta c))}{N_0 \Delta c}, \quad (14)$$

here $N(c_2^{(ik)}(z) \geq c_2)$ is the quantity of points in a given horizontal plane z , at which current concentration $c_2^{(ik)}$ is higher than c_2 , $N_0(z)$ is the total number of the points in the plane. The c_2 runs through a sequence of M numbers:

$$c_2 = (0, \quad 1, \quad 2, \quad \dots, \quad M-1)\Delta c,$$

where $M\Delta c = 1$; in our computations, $M=100$.

When the initial concentration array is used, because of circuit features of calculation of concentration in separately taken cell the maximal values $F(c_2)$ are achieved basically (inside TMZ) near to borders of an interval of values of concentration, that is, at $c_2 \approx 0$ or ≈ 1 . Thus inside an interval $0 < c < 1$ values $F(c_2)$ are small, that is, the integral is gathered basically at edges of an interval. Near to border TMZ, adjoining to heavy substance, $F(c_2)$ looks like δ -function concentrated at $c_2 \approx 1$.

However, with use of averaging of an initial concentration array on squares with the side n_0 , in calculation for variant $N=1.6107$, $n=10$ with increase n_0 from 2 up to 4 it is observed (as shows rice 12) fast approach to certain established kind $F(c_2)$, not dependent from n_0 . Its characteristic feature is almost uniform distribution on c_2 inside TMZ, that is, $F(c_2) \approx 1$ - and the integral is gathered almost uniformly on all interval.

The form of the function is similar for other n .

References

1. Youngs D.L., Numerical simulation of mixing by Rayleigh-Taylor and Richtmyer-Meshkov instabilities, Laser and Particle Beams, vol 12, no. 4, pp. 725-750 (1994).
2. Sinkova O.G., Stadnik A.L., Statsenko V.P., Yanilkin Yu.V., Zhmailo V.A., Three-Dimensional Direct Numerical Simulation of Gravitational Turbulent Mixing, 6th Inter. Workshop on the Physics of Compressible Turbulent Mixing, Marseille France, pp.470-479 (1997).
3. Stadnik A.L., Shanin A.A., Yanilkin Yu.V. Eulerian code TREK for computing 3D gas-dynamic multicomponent medium flows// VANT. Ser. Mat. Modelir. Fiz. Protsessov, No.4 (1994).
4. Read, K.I. Experimental investigation for turbulent mixing by Rayleigh-Taylor instability //Physica D12, 45 (1984).
5. Youngs, D.L. Modeling turbulent mixing by Rayleigh-Taylor instability //Physica D37, 270 (1989).

6. Yu.A.Kucherenko, L.I.Shibarshov, V.I Chitajkin et al. Experimental study of the gravitational turbulent mixing self-similar mode //3-rd International Workshop on the physics of compressible turbulent mixing, pp.345-356 (1991).
 7. Linden P.F., Redondo J.M., Youngs D.L., Molecular mixing in Rayleigh-Taylor instability, J. Fluid Mech, vol.265, pp.97-124, (1994).
 8. Youngs, D.L., Three-dimensional numerical simulation of turbulent mixing by Rayleigh-Taylor instability, Phys. Fluids, A3, 1312 (1991).
- Kucherenko Yu.A., Shestachenko O.E., Piskunov Yu.A., Sviridov E.V., Medvedev V.M., Baishev A.I. Experimental study for self-similar mode of different-density gas mixing in the Earth's field gravity. Paper presented at the 6th Zababakhin Scientific Talks, 24-28September 2001, Snezhinsk, Russia.

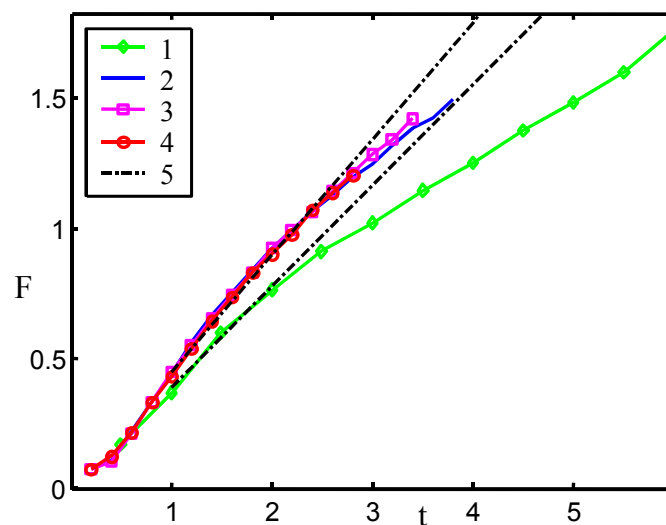


Fig. 2. Function F of TMZ width L versus t ;
our computations: 1 – $n=3$, 2 – $n=10$, 3 – $n=20$, 4 – $n=40$, 5 – by α taken in [7]

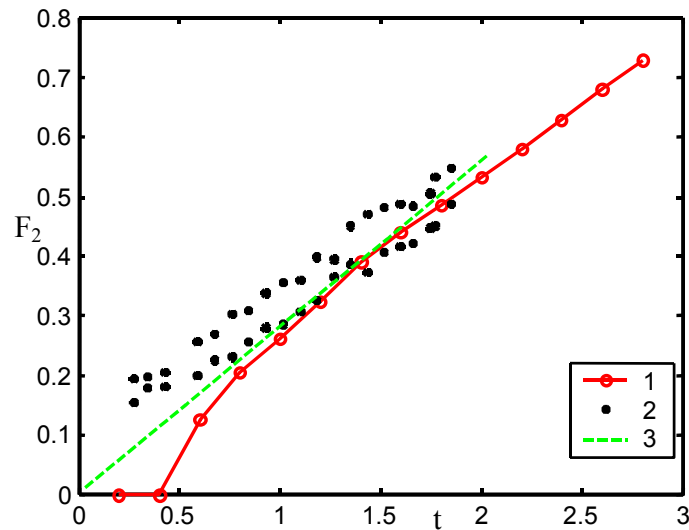


Fig. 3. Function F_2 of coordinate z_2 of heavy liquid penetration into light liquid versus time t : 1 – our computation for $n=40$, 2 – minimum and maximum values measured in ref. [9] for $n=36.5$, 3 – by $\alpha_2=0.078$ taken in [9]

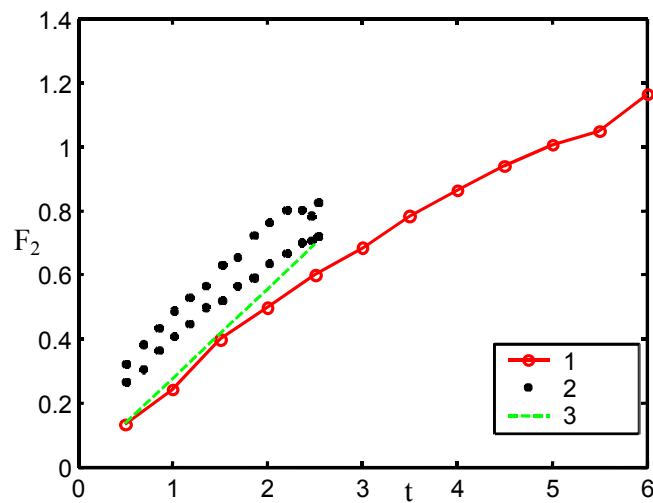


Fig. 4. Function F_2 of coordinate z_2 of heavy liquid penetration into light liquid versus time t : 1 – our computation for $n=3$, 2 – minimum and maximum values measured in ref. [9] for $n=3.65$, 3 – by $\alpha_2=0.078$ taken in [9]

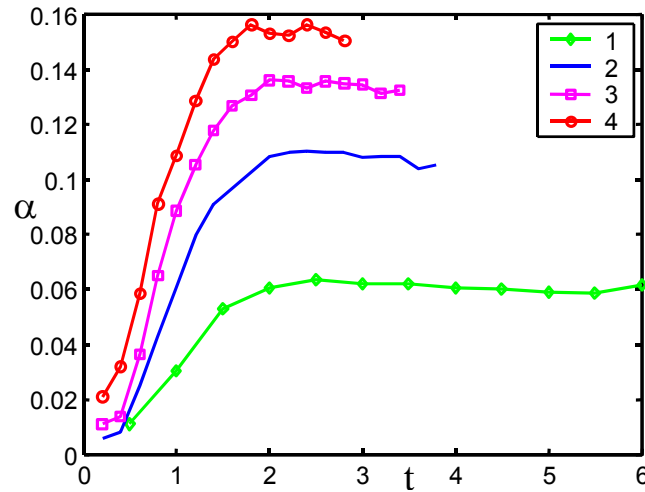


Fig. 5. Scaled TMZ width versus time. The notations are like those in Fig.2

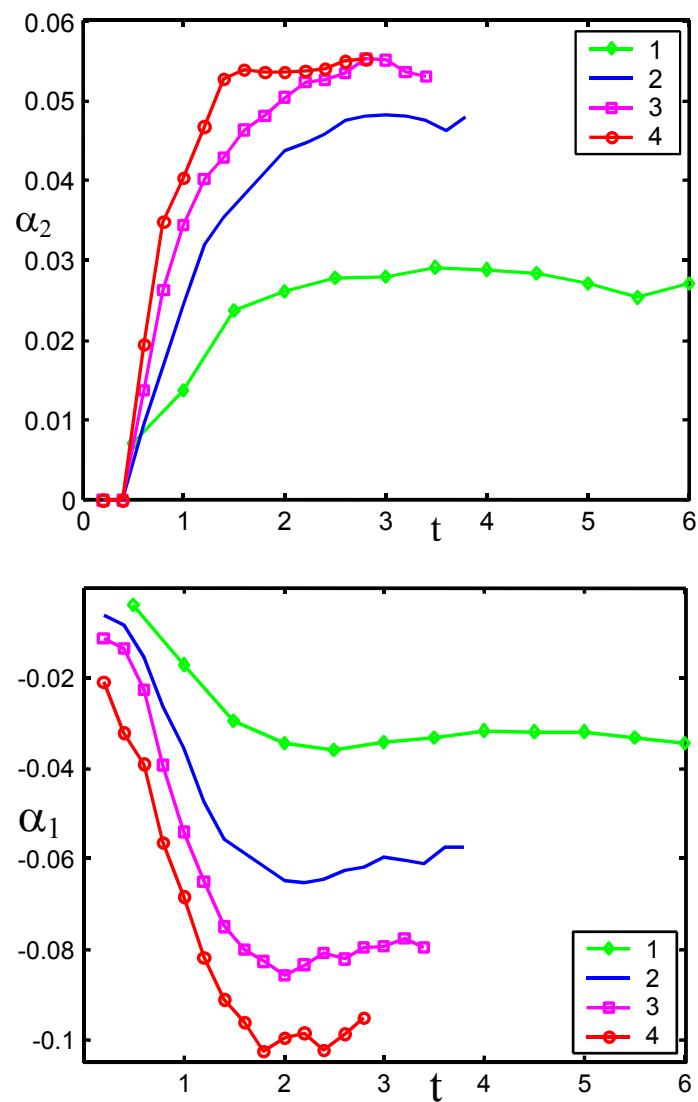


Fig. 6. Scaled TMZ boundary coordinate in light material (α_1) and heavy material (α_2) versus time. The notations are like those in Fig.2

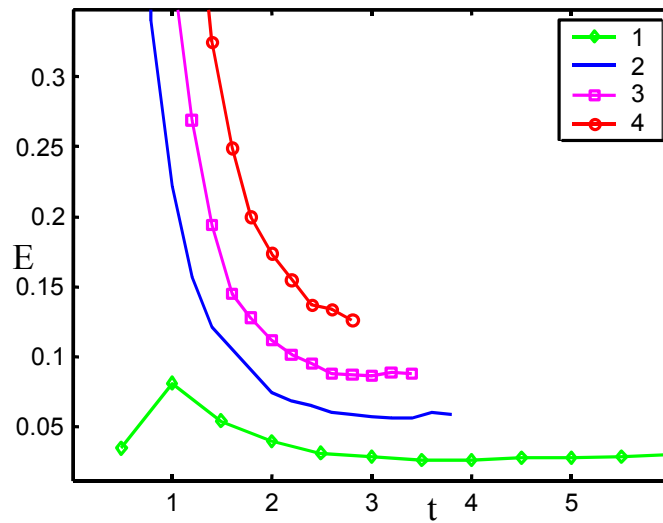


Fig. 7. TMZ maximum scaled turbulent energy versus time.
The notations are like those in Fig.2

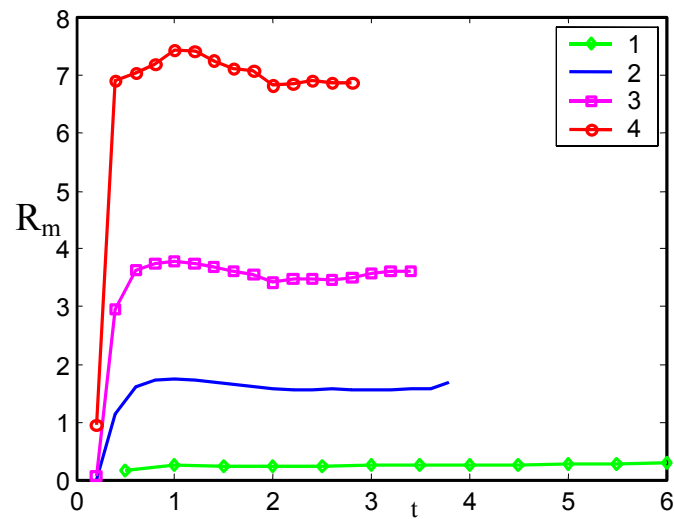


Fig. 8. TMZ maximum density pulsation function versus time.
The notations are like those in Fig.2

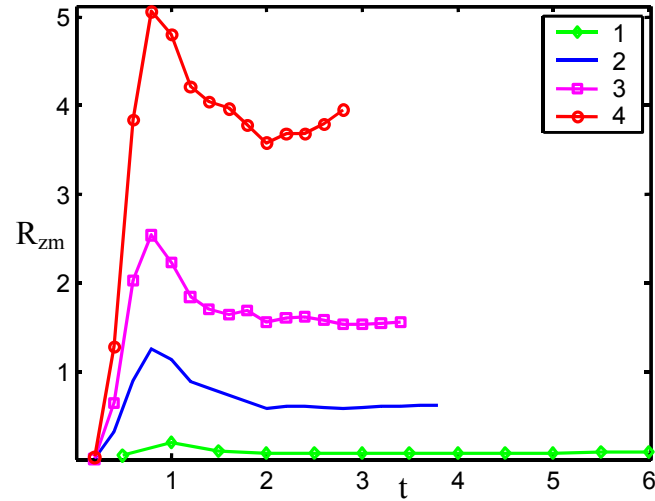


Fig. 9. TMZ maximum turbulent mass flow versus time. The notations are like those in Fig.2

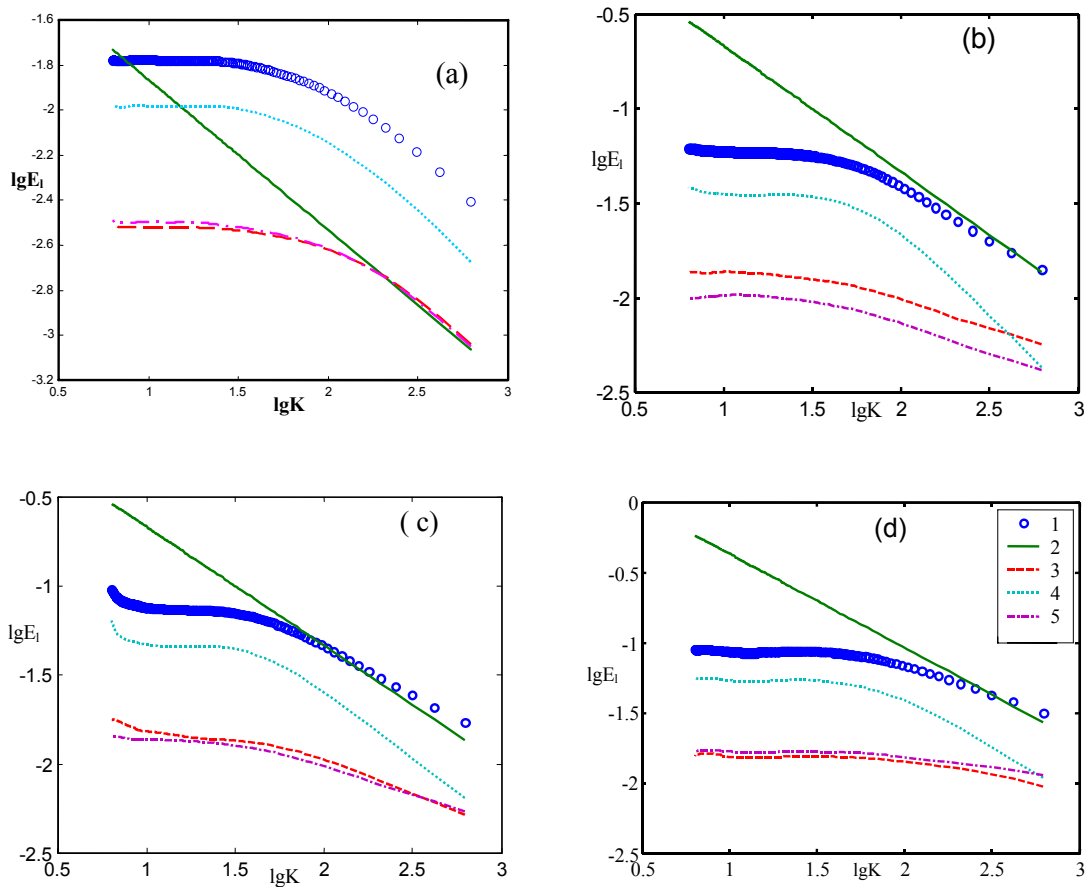


Fig. 10. Velocity pulsation spectrum,
 (a) $n=3$, $t=3.5$, $\zeta=-0.076$, (b) $n=10$, $t=2.5$, $\zeta=-0.076$, (c) $n=20$, $t=2.5$, $\zeta=0.055$,
 (d) $n=40$, $t=2$, $\zeta=-0.36$; 1 - E_l , 3 - E_{xxl} , 4 - E_{zzl} , 5 - E_{yy} ; 2 - Kolmogorov spectrum.

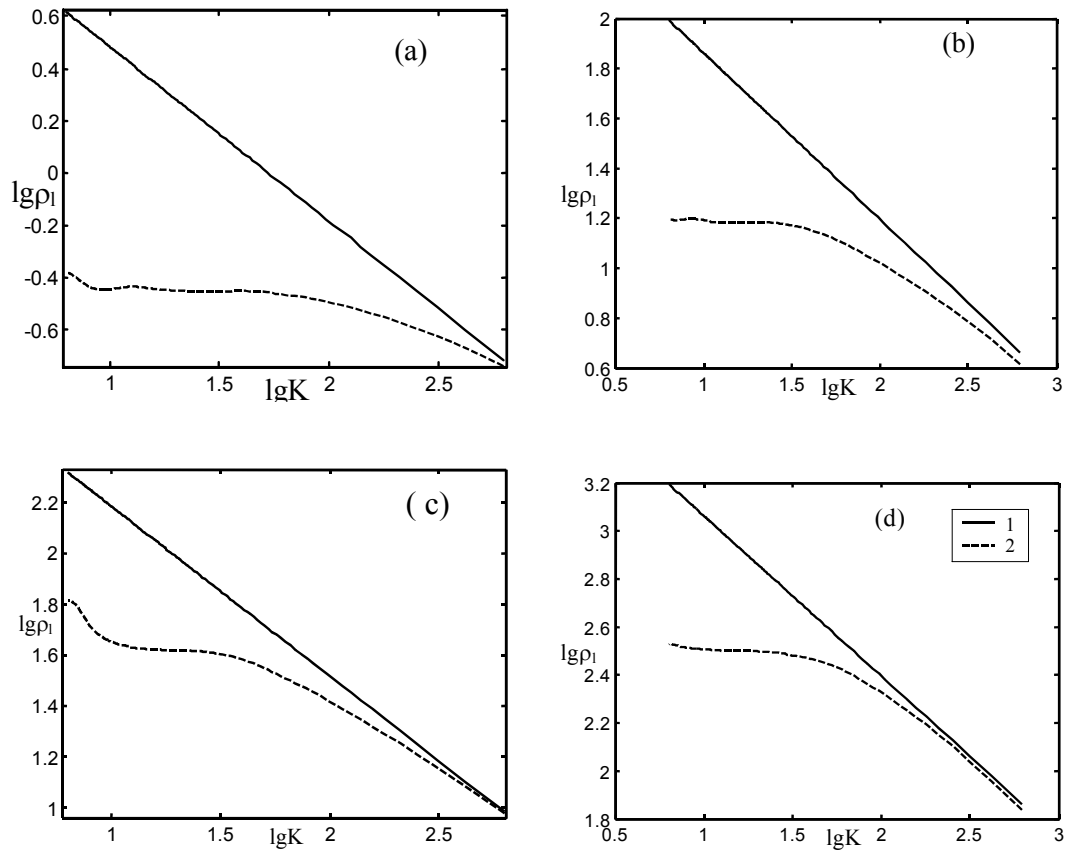


Fig. 11. Density pulsation spectrum,
 (a) $n=3, t=4.5, \zeta=0.137$, (b) $n=10, t=2.5, \zeta=0.236$, (c) $n=20, t=2.5, \zeta=0.22$,
 (d) $n=40, t=1.8, \zeta=0.19$; 1 – ρ_1 , 2 - Kolmogorov spectrum.

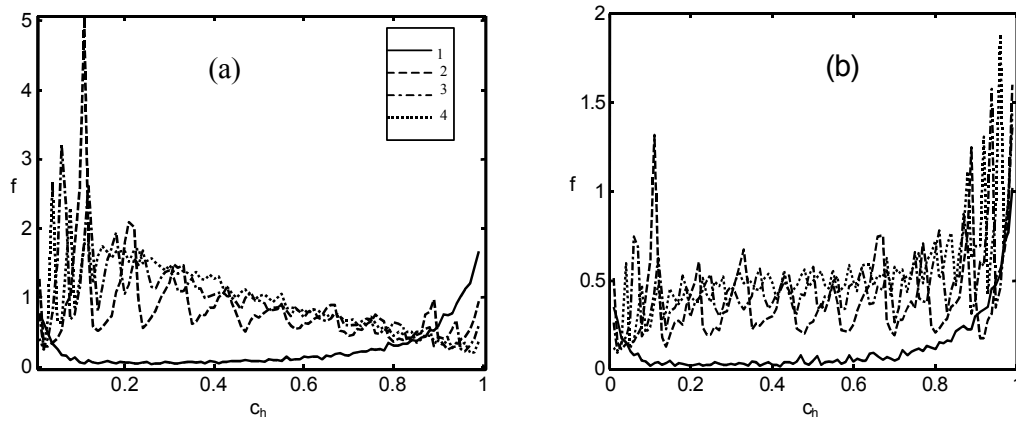


Fig. 12. Heavy material mass concentration probability density function, $n=10, t=2$;
 $M=100$. 1 – $n_0=1$, 2 – $n_0=2$, 3 – $n_0=3$, 4 – $n_0=4$; a) $\zeta = -0.187$, b) $\zeta = 0.41089$.